Correlations between Reaction Product Yields as a Tool for Probing Heavy Ion Reaction Scenarios

W. Gawlikowicz[1,2], D.K. Agnihotri[1], S.A. Baldwin[1], W.U. Schröder[1],
J. Tõke[1], R.J. Charity[3], D.G. Sarantites[3], L.G. Sobotka[3], R.T. deSouza[4],
T. Barczyk[5], K. Grotowski[5], S. Micek[5], R. Płaneta[5], and Z. Sosin[5]

[1]*Departments of Chemistry and Physics,*
University of Rochester, Rochester, NY 14627, USA

[2]*Heavy-Ion Laboratory, Warsaw University, Warsaw, Poland*

[3]*Department of Chemistry, Washington University, St.Louis , MO 63130, USA*

[4]*Department of Chemistry, Indiana University, Bloomington, IN 47405, USA*

[5]*Institute of Physics, Jagellonian University, 30-059 Krakøw, Poland*

Abstract

Experimental multidimensional joint distributions of neutrons and charged reaction products were analyzed for $^{136}Xe + ^{209}Bi$ reactions at E/A = 28, 40, and 62 MeV, and were found to exhibit several different types of prominent correlation patterns. Some of these correlations have a simple explanation in terms of the system excitation energy and pose little challenge to most statistical decay theories. However, several other types of correlation patterns are difficult to reconcile with some, but not other possible reaction scenarios. In this respect notable are correlations between the average atomic number of intermediate-mass fragments, on the one hand, and light particle multiplicities, on the other hand. This kind of multi-particle correlations provides a useful tool for probing reactions scenarios, which is different from the traditional approach of interpreting inclusive yields of individual reaction products.

PACS numbers: 25.70.Pq,25,70.Mn

I. INTRODUCTION

Over the last 20 years, or so, considerable effort has been made both, experimentally and theoretically, to explore heavy-ion reaction dynamics and to understand the production scenarios of various products. As a result of this effort, a consensus has emerged as to the general collision scenario prevailing at low bombarding energies and, perhaps, also at the lower part of the Fermi-energy domain. In this "consensus" domain, the projectile and target are believed to proceed in a way of a dissipative collision, where they form transiently a revolving dinuclear complex and convert an ever increasing (with time passing) part of the kinetic energy of relative motion into intrinsic thermal and rotational energies. Phenomena of energy and angular momentum dissipation and mass transfer are thought to be effected mainly by means of stochastic nucleon exchange between the projectile-like and target-like constituents. Subsequently, the dinuclear complex reseparates under the combined action of Coulomb and centrifugal forces, and the projectile- (PLF) and target-like (TLF) fragments are set free to proceed on their individual Coulomb trajectories. Furthermore, the PLF and TLF are believed to emerge from the dissipative collision excited and thermally equilibrated and, accordingly, to decay statistically. Superimposed on the above simple scenario, but not interfering with it to any significant extent, is pre-equilibrium emission of neutrons and light charged particles (LCP), occurring mostly at early stages of the collision history. It is important to note that instrumental in arriving at the above "consensus" picture were observations of individual product yields and, specifically, of patterns in the yield distributions characteristic of the inferred "consensus" scenario. For example, a notorious pattern is that seen in typical Wilczyński plots [1] of PLF yield as a function of PLF kinetic energy and deflection angle.

At higher bombarding energies, up to $E/A = 62$ MeV, the underlying general dissipative collision scenario still appears to be consistent with a variety of experimental observations made at energies close to the interaction barrier [2]. However, here a consensus is still lacking as to the dominant production mechanisms of the observed light and intermediate-mass reaction products. To some extent, this is so because of expectations of an increased role of two-body interactions and of increased preequilib-

rium emission, possibly including emission from the dynamically unstable interfragment "neck-like" structure [3–5]. But more importantly, it is so because of the observation of copious production of intermediate-mass-fragments (IMFs), which exhibits certain aspects of statistical independence [6, 7] but appears difficult to reconcile with classical scenarios of a statistical decay of an equilibrated nuclear system. A number of unconventional statistical approaches have been developed [8–10] to address the shortcomings of traditional models of statistical particle emission when applied to IMFs. On the other hand, several experimental studies [11–15] have concluded a dominantly non-equilibrium mode of IMF production.

The failure to reach a consensus at these higher energies may well point to inherent limitations of a "one-dimensional" analysis based on yields of individual species of reaction products and, thus, call for an extended analysis scheme involving various correlations between the production patterns of different species, such as neutrons, LCPs, IMFs, PLFs, and TLFs.

With the potential probing value of such correlations in mind, a series of experiments were performed, in which all of the many types of products were measured simultaneously, event-by-event. More specifically, in these experiments both, neutrons and charged reaction products were measured with 4π angular coverage using the Rochester *Superball* or *RedBall* neutron calorimeter/multiplicity meters in combination with one of the available 4π charged-product detector arrays (MSU $MiniBall$, Washington University $DwarfBall/Wall$ and $MicroBall$). Additionally, PLFs were measured at forward angles, also with high geometrical efficiency resulting from their strong kinematical focussing.

The present study focuses on experimental data on ^{209}Bi + ^{139}Xe reactions at E/A=28, 40, and 62 MeV and aims at evaluating the significance of three types of prominent correlation patterns observed in multidimensional joint distributions of neutrons, LCPs, IMFs, and PLFs as a tool of probing the underlying reaction scenario and, by implication, the production mechanisms of these species. The correlations considered include those between the neutron and charged particle multiplicities, between the average size of IMFs and the joint neutron and LCP multiplicity, and between the average size of PLFs and the joint neutron and LCP multiplicity.

II. ESSENTIALS OF THE EXPERIMENTAL SETUP

The experiment was performed at the National Superconducting Cyclotron Laboratory of the Michigan State University. The beams of ^{136}Xe ions from the K1200 cyclotron, with energies of E/A = 28, 40, and 62 MeV were focussed on a self-supporting 3.5-mg/cm^2 thick ^{209}Bi target placed in the operational center of the detector setup. The latter consisted of two 4π detector systems, the Washington University charged-particle detector array, $DwarfBall/Wall$ [16] and one of the University of Rochester neutron calorimeter/multiplicity meters, $SuperBall$ [17] or $RedBall$. Additionally, two position-sensitive silicon-detector telescopes were placed at forward angles, so as to cover an angular range encompassing the anticipated grazing angle ($\theta_{Grazing}$= 4.48^o, 3.90^o , and 2.91^o, for 28, 40, and 62 MeV/nucleon reactions, respectively). The $Dwarf$ array provided for a reliable Z identification for atomic numbers up to Z=35, but also for the energy and emission angle measurement [18]. The $SuperBall$ provided for a high-efficiency event-by-event measurement of neutron multiplicities and of summed kinetic energy of neutrons, in five angular bins. Since the mean detection efficiencies for the relatively weak components of high-energy preequilibrium neutrons and protons are much smaller [SuperBall,Djerroud] than for the less energetic, statistically emitted particles, the multiplicities measured for neutrons and LCPs reflect mainly the thermal excitation energies of the emitter nuclei.

The forward-angle telescopes provided for Z identification of projectile like fragments, along with the energy and angle measurement. They were also sensitive to intermediate-mass fragments. In all cases, the "minimum bias" trigger for the data acquisition was provided by one charged particle registered by any of the detectors. While even elastic scattering of projectiles was measured in the experiments, a PLF coincidence was not required in the definition of the minimum bias trigger. Thus the experimental setup allowed one to obtain an almost complete characterization of individual reaction events in terms of product identification, their yields, and corresponding kinematical parameters.

III. THEORETICAL MODELING OF VARIOUS REACTION SCENARIOS

The ultimate goal of modeling of any particular reaction scenario is to obtain model predictions for experimentally measured patterns in reaction product yields, so the latter can be used to verify the consistency of, or to falsify the scenario under scrutiny. Given the complex nature of the processes leading from the heavy-ion collision to the detection of products, the modeling is in practice always a multi-step endeavor involving both, "fundamental" modeling of physical phenomena of interest and a more technical in nature modeling of the detection processes. Quite generally, the latter is free of hypotheses and includes modeling of the geometrical and electronic acceptance (thresholds, dynamical ranges) of the detector setup to reaction products, but may also include calculations of multi-particle Coulomb trajectories from the moment in time when the particles are set free in the fundamental theoretical models to the moment they reach their respective asymptotic trajectories.

In heavy-ion reactions at low and intermediate bombarding energies, the fundamental theoretical modeling itself is typically a two-step process, with the first step aiming at describing the collision dynamics and the second one aiming at describing the decay of the primary reaction products. Generally, the outcome of such simulation calculations depends on assumptions made in both steps, which tends to obscure an interpretation of possible discrepancies between the predictions and the experimental observations. Therefore, of special value are predictions for patterns that are uniquely sensitive to one of the two steps but not to the other.

In the present study, two theoretical codes were used alternately to model the dynamical, interaction stage of the collision, while two other codes were used alternately to model the subsequent statistical decay of the primary products emerging from the interaction stage with the dynamical model predictions for product mass and atomic numbers, excitation energies and spins. And so, the interaction stage was modeled using either the classical transport code CLAT [19], based on a stochastic nucleon exchange model NEM [20] or the Quantum Molecular Dynamics (QMD) code CHIMERA [21], accounting in a better detail for the two-body interactions. The version of the CHIMERA code used [21] included isospin dependent nuclear interactions, and calculations were performed

for the time interval from 0 to up to 300 fm/c assuming a soft EOS ($K \approx 200MeV$) with symmetry energy strength coefficient corresponding to an ASY-STIFF EOS (C = 31.4 MeV) [22].

The statistical decay of the primary fragments predicted by the dynamical models of the interaction stage was then modeled using either the equilibrium-statistical, sequential decay code GEMINI [23] or the (pseudo-microcanonical) statistical multifragmentation code SMM [8].

Note, that the physical scenario nominally implemented in the code CLAT may be not too an accurate representation of the interaction at higher bombarding energies. What matters in the present study, however, is that it provides still a surprisingly good effective parametrization of the interaction, and in particular of the dissipation function. The code SMM, on the other hand, as a matter of principle does not represent any realistic physical scenario, that can be supported by generally accepted theories of nuclear matter. Therefore, also this code is here viewed merely as providing a reasonably good effective parametrization of the statistical decay of excited nuclear systems.

A multi-particle Coulomb trajectory calculation routine [24] was applied to the end products predicted by the "standard" GEMINI code [23], making use of the (statistical) timing, spatial locations, decay axes, and relative energies of all (binary) decays along the deexcitation cascade. This kinematic "after-burner" allowed one to calculate energies and asymptotic emission angles of all reaction products.

The results of model calculations were subsequently passed through a routine calculating the response of the $DwarfBall/Wall$ and $SuperBall$ 4π detector systems to each and every reaction product predicted by model calculations. The routine accounted for the geometrical acceptance and the detection efficiency of all detectors for various particle species. The efficiency of the $SuperBall$ was calculated using a version of the well-known code DENIS [25]. This procedure of converting "generic" theoretical predictions into custom predictions for a given detection setup is often called "filtering". The "filtered" model predictions, is what can be meningfully compared to the experimental data.

IV. EXPERIMENTAL RESULTS AND ANALYSIS

In the following subsections, three types of prominent correlations between the yields of four distinct classes of reaction products, neutrons, LCPs, IMFs, and PLFs are discussed and analyzed in terms of various reaction scenarios, represented by pairs of theoretical models discussed further above.

A. Neutron and LCP Multiplicity Correlation Patterns

It is well known from the literature [26–28] that the joint multiplicity distributions of neutrons and light charged particles can be used as measures of kinetic energy dissipation achieved in individual reaction events. Such a distribution for the $^{136}Xe+^{209}Bi$ reaction at E/A = 40 MeV is shown in the upper panel of Fig. 1 in form of a (logarithmic) contour plot, while the respective distributions expected for different interaction/decay scenarios are shown in the other panels. As seen in the first panel in Fig. 1, the experimental two-dimensional joint multiplicity distribution features a prominent intensity ridge with a crest line running first parallel to the neutron multiplicity axis and then, at $m_n \approx 20$, turning away from this axis, to continue along a line running at an angle with respect to the coordinate axes. Such a behavior has a natural explanation in phase-space based statistical decay models, which favor strongly neutron emission at low excitation energies, hence the section of ridge parallel to the m_n axis. At higher excitation energies, when the nuclear temperature becomes comparable to the height of the Coulomb barrier for the emission of LCPs, emission of the latter can successfully compete with neutron emission.

A somewhat less conspicuous feature of the joint neutron-LCP multiplicity distribution is the presence of a "pass" in the ridge at around $(m_{LCP}, m_n) \approx (5, 28)$. Note that both terms, the "pass" and the "ridge" refer to a hypersurface in the three-dimensional space spanned on particle multiplicities and on the number of events. Mathematically, the "pass" is a saddle point on this hypersurface. As the distance along the ridge from the origin of the plot represents reasonably well excitation energy in the system [27], the presence and the location of the "pass" are reflections of a particular mix of dissipative and conservative forces acting between the collision partners. More specifically, they are

reflections of the form of dissipation function, i.e., of the impact-parameter dependence of the dissipated energy. Because of this, the location of the "pass" can possibly be used to validate effective interactions employed in collision codes, a task that is beyond the scope of the present study.

The experimental crest line is shown in all panels of Fig. 1, liberally extrapolated beyond the high-multiplicity peak of the ridge. Note, that the ridge cannot be uniquely defined mathematically beyond that peak.

As seen in Fig. 1, all theoretical scenarios, represented here by combinations of model codes "CLAT + GEMINI" (one-body interaction and sequential decay), "CLAT+SMM" (one-body interaction followed by the decay of systems at "freezeout" configurations), and "QMD+GEMINI" (one- and two-body dynamics followed by sequential decay of primary products), tend to reproduce the general appearance of the joint multiplicity distribution. However, there are significant differences as to the quality of the resemblance

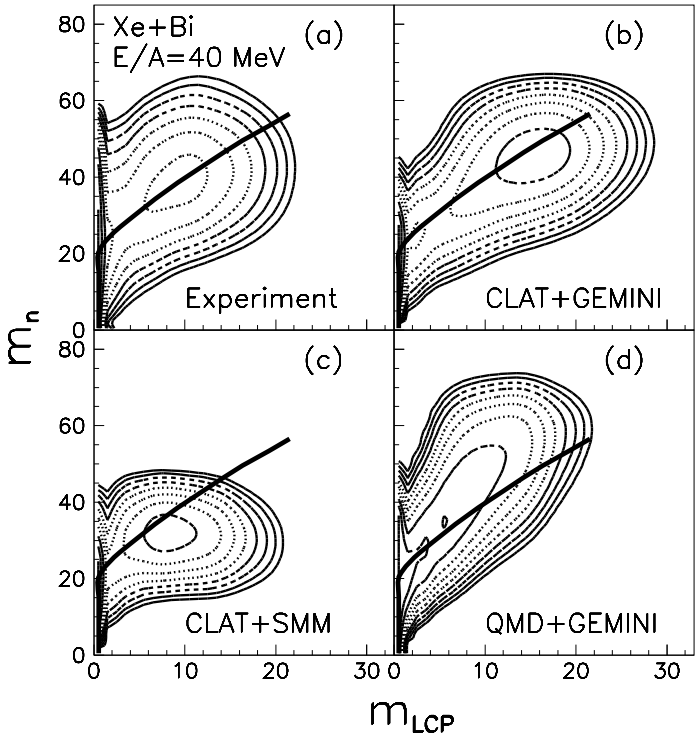

FIG. 1: Logarithmic (base 2) contour plots of experimental (a) and various model (b - d) joint distributions of neutron (m_n) and light-charged particle (m_{LCP}) for $^{136}Xe + ^{209}Bi$ reaction at E/A = 40 MeV.

between the experimental plot, on the one hand and various theoretical predictions, on the other hand.

It appears that the least complex calculations based on the codes CLAT [19] and GeminiGEMINI [23] provide for the best agreement with experimental observations, as far as the location of the crest line of the yield ridge and the location of the "pass" in the ridge are concerned. However, it still fails to reproduce the location of the peak at high particle multiplicities. In model calculations, this latter location depends on "dissipation function" describing the way in which degree of effected kinetic energy dissipation depends on the impact parameter. However, it is not clear whether the observed discrepancy between the actual and model locations of the high-multiplicity peak is due partially or wholly to a flawed modeling of the dissipation function by the code CLAT with its particular implementation of the stochastic nucleon exchange model, NEM. This is so because the CLAT + GEMINI combination neglects entirely the role of an effective intermediate-velocity source (IVS) which emits particles, and especially IMFs with higher average kinetic energies than the purely thermal energies characteristic of equilibrated PLF and TLF sources. Inclusion of preequilibrium emission and production of IMFs would result in shifting the peak in theoretical (CLAT + GEMINI) yield ridge in Fig. 1 towards lower particle multiplicities, bringing it to a better agreement with the experimental one.

As seen in the corresponding panel in Fig. 1, a combination of the codes CLAT and SMM predicts a saturation in neutron multiplicity not observed experimentally, such that the model calculations "misplace" the crest line itself. Here, not only the location of the high-multiplicity peak in the joint neutron and LCP multiplicity distribution, but also the location of the "pass" in the ridge disagree markedly with the experimental ones. Although these facts do not necessarily disqualify the SMM as a viable model, they point to specific model deficiencies in the description of relative neutron and LCP yields and should help in devising corrections to the model that remedy this deficiency.

As seen in the bottom right panel in Fig. 1, the QMD + GEMINI calculations largely fail to reproduce the "topography" of the yield ridge such that not only they misplace the crest line, but also miss the "pass" in the ridge and the high-multiplicity peak altogether. Clearly, these model calculations over-predict the emission of neutrons compared with

LCPs, which may be indicative of the neutron yield being strongly affected by dynamical emission during the interaction stage of the collision. If so, it would be a deficiency that, apparently, cannot be remedied by simple *ad hoc* corrections to the QMD code CHIMERA [21]. Therefore, one may conclude tentatively that at $E/A = 40$ MeV, the collision dynamics is still largely governed by one-body dynamics and that the effects of direct nucleon-nucleon interactions are still too weak to justify a "universal" use of QMD logic for evaluating individual yields of all reaction products. However, the possibility that QMD provides a reasonably good description of the interaction stage for a limited range of impact parameters cannot be excluded.

In conclusion of this section, one must note that the "topography" of the yield distribution as a function of neutron and LCP multiplicities, which features prominently a "ridge", a "pass" and a "peak" at high particle multiplicities may serve not only as a primitive tool of validating theoretical models but also as a more nuanced tool of actually revising and up-grading these models.

B. Correlations between Average Fragment Sizes and the Joint Multiplicity of Neutrons and LCP

In recent years, prominent correlations between the average sizes of IMFs and the joint multiplicity of neutrons and protons have been discovered [2], which were found also to exhibit non-thermal scaling, such that they depend on the bombarding energy.

Such correlations are illustrated for three bombarding energies in Fig. 2, each in form of a contour diagram of the average atomic number $< Z_{IMF} >$ of IMFs plotted *versus* the associated neutron and LCP multiplicities. No bias has been imposed on the distribution of IMFs admitted in these plots other than $3 \leq Z_{IMF} \leq 10$. This segment of the product Z distribution is well separated from the domains of PLFs, their evaporation residues and their fission fragments. As seen in these plots, the average size of the IMFs produced is correlated prominently with the joint multiplicity of neutrons and LCPs, which reflects the dissipated and "thermalized" energy in heavy-ion collisions [26–28]. Hence, larger IMF sizes are associated with higher excitation energies. Interestingly, higher excitation energies also lead to higher multiplicities M_{IMF} of IMFs, which are

mostly emitted [2] at excitation energies associated with the "central collision bump" in the joint neutron/LCP multiplicity distribution mentioned previously. The clear "equi-size" contour lines running almost perfectly parallel to each other appear to coincide with lines of constant excitation energy. They are a unique experimental manifestation of what is a trivial anticorrelation of neutron and LCP multiplicities in statistical decay models such as, e.g., GEMINI [23]. Note that this kind of multi-particle correlation involves three independently measured quantities, neutron and LCP multiplicities and the atomic numbers of IMFs and.

Importantly, as is clear from the comparison of the three panels in Fig. 2, the contour lines of equal $< Z_{IMF} >$ shift systematically toward higher neutron and LCP multi-

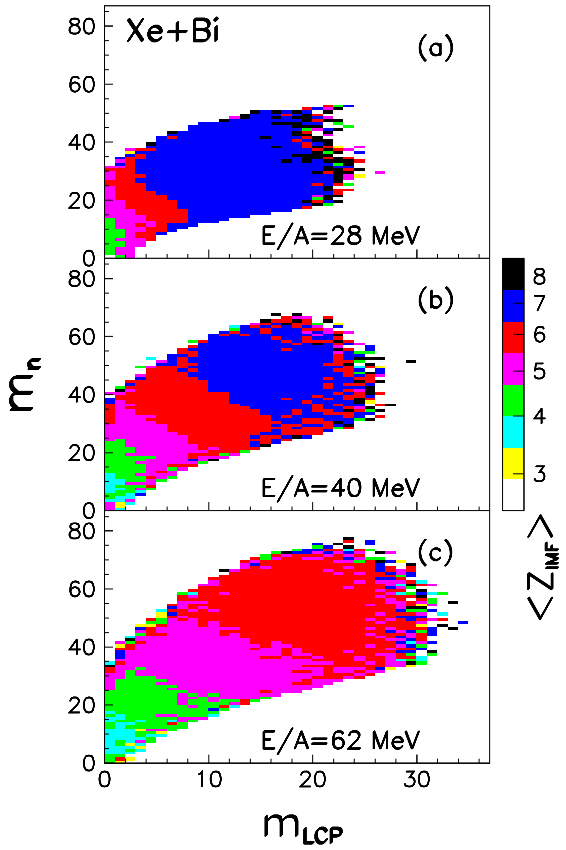

FIG. 2: (Color online) Logarithmic contour plot of average atomic number of IMFs, $< Z_{IMF} >$, as a function of associated neutron and LCP multiplicities as observed in $^{136}Xe + ^{209}Bi$ reactions at E/A = 28 MeV (top panel), E/A = 40 MeV (middle panel), and E/A = 62 MeV (bottom panel). Here, $3 \leq Z_{IMF} \leq 16$.

plicities as bombarding energy increases, which suggests that they do not scale directly with thermal excitation energy. This observation may then be indicative of a significant portion of IMFs being produced in dynamical processes. Indeed, this kind of scaling of the average size of IMFs is consistent with scaling according to the size of the overlap region between projectile and target or possibly the size of the neck-like structure formed transiently between the interacting PLF and TLF. Such a conclusion is based on the observation that for higher bombarding energies a comparatively smaller overlap region leads to the same given excitation energy than at lower bombarding energies, hence the shift of contour lines toward higher excitation energies but same overlap. While preequilibrium emission on neutrons and LCP's may also cause some shift of contour lines with bombarding energy, this shift is relatively small given the generally moderate multiplicity of preequilibrium particles. In fact, the presence of preequilibrium emission is expected to shift the lines in the direction opposite to that observed, as now the same thermal excitation energy will correspond to higher particle multiplicities.

Results of attempts to reproduce the observed correlations at E/A=40 MeV by three reaction scenarios are illustrated in Fig. 3 along with the experimental distribution (left top panel). Model calculations included always the "experimental filter" accounting for the response of the detector setup. As seen in the second panel in the first row, the combined "CLAT + GEMINI" results only resemble the data in so far as the m_n-m_{LCP} correlation is concerned, but misses the size correlation pattern, consistent with the presence of the dynamical component in IMF yield as discussed above. This is also not surprising in view of the fact that very few IMFs are expected within the framework of these two models.

The left panel in the bottom row of Fig. 3 illustrates the failure of the statistical multifragmentation model SMM [8] to account for a prominent experimental correlation pattern. While based on the argument regarding the presence of a dynamical component in the IMF yield one would not expect a particularly good agreement with experiment in this case, the correlations predicted for the CLAT + SMM scenario are to a good extent "orthogonal" to those actually observed. This may be taken as indicative of a statistical multi-fragment breakup of an equilibrated system such as contemplated by SMM playing little, if any role in IMF production in the bombarding energy range

considered and suggesting that the IMF production occurs, perhaps, with no meaningful competition from particle decay channels.

The right panel in the bottom row of Fig. 3 illustrates predictions by the QMD code CHIMERA [21] complemented by code GEMINI and the Coulomb trajectory "after-burner" [24]. Even though the CHIMERA scenario appears inconsistent with the correlation pattern seen in the joint distribution of neutron and LCP multiplicities, it may still be responsible for IMF production in a limited range of impact parameters. This is possible in view of a strong indication that the IMFs, unlike neutrons and LCPs, are to a large extent produced in dominantly dynamical processes, expected to be well described

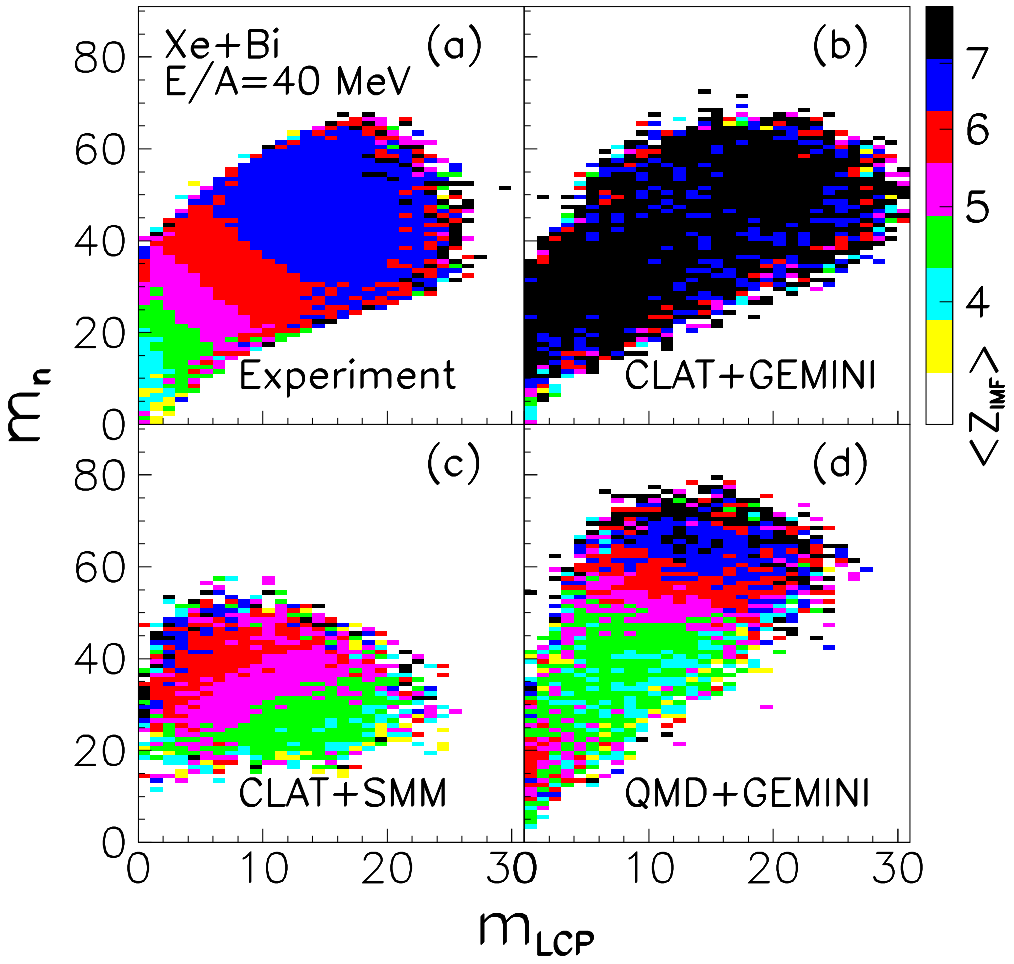

FIG. 3: (Color online) Logarithmic contour plots of average atomic number of IMFs, $< Z_{IMF} >$ as a function of associated neutron and LCP multiplicities m_n and m_{LCP}, as predicted by three sets of model calculations for E/A=40 MeV (see text).

by QMD type of codes. Indeed, as seen in the respective panel in Fig. 3, CHIMERA is capable to correctly render the trends observed experimentally and, most notably, the increase of average IMF size with increasing neutron and LCP multiplicities. In this respect, it would be highly desirable to compare CHIMERA predictions to correlations experimentally observed for a range of bombarding energies.

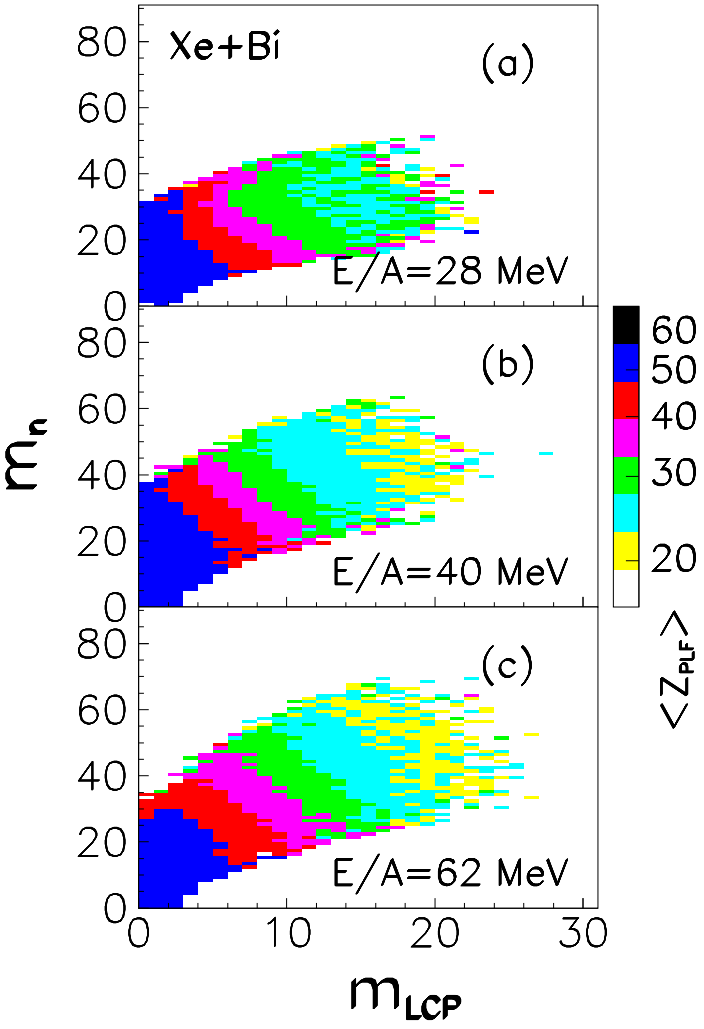

FIG. 4: (Color online) Logarithmic contour plot of average atomic number of the detected PLF, $< Z_{PLF} >$, as a function of associated neutron and LCP multiplicities, as observed in $^{136}Xe + ^{209}Bi$ reaction at E/A = 28 MeV (top), 40 MeV (middle), and 62 MeV (bottom).

C. Correlations between the Size of PLF and the Joint Multiplicity of Neutrons and LCP

Figure 4 illustrates correlations between the average size of the PLF and the associated joint multiplicity of neutrons and LCPs, as observed at three bombarding energies of E/A=28 MeV (top panel), 40 MeV (middle panel), and 62 MeV (bottom panel). As seen in Fig. 5, these correlations appear easy to understand within a prevailing scenario of a dissipative collision followed by statistical and sequential decay of primary PLF and TLF, as modeled by a two-step $CLAT + GEMINI$ calculation. However, they can also be understood within the frameworks of the combined $CLAT + SMM$ and of the combined $QMD + GEMINI$ scenarios. It appears then that this type of correlation is of a lesser value as far as probing the more detailed interactions scenario is concerned. Yet the fact that they do not contradict conclusions reached further above is in itself encouraging.

V. SUMMARY

The present work has shown that certain prominent correlations observed between the yields of different reaction products can be used to probe the underlying collision and decay scenario and, hence serve as a guidance in devising models of heavy-ion collision and decay of the excited primary products. Already the simple correlation pattern between the multiplicities of neutrons and LCPs tends to exclude dynamical QMD models as describing the overall collision scenario in the bombarding energy domain considered. It appears that even at $E/A = 62MeV$ the reaction dynamics is still largely dominated by one-body interactions with lesser propensity to a preequilibrium release of particles and fragments than exhibited by a two-body interaction dominated scenario.

Concerning IMF production, the relevance of a break-up state as modeled in an SMM-like freezeout scenario appears to be strongly contradicted by the prominent experimental trends, and at this time there seems to be no obvious remedy for this deficiency of SMM. The latter observation is perhaps related to the recently reported [29] inconsistency of SMM predictions with the IMF production observed in a spallation reaction, whereas the same data were well explained by GEMINI calculations. In that work [29],

an intranuclear cascade code (INC) was used to simulate the interaction stage of the process.

In contrast, but in agreement with other recent works [11–14], the present study suggests that IMF production in heavy-ion reactions is dominated by dynamical processes resembling QMD-like scenarios. This conclusion is largely based on the bombarding-energy dependence of the experimental correlations between the average size of IMFs and the joint neutron and LCP multiplicity reported so far in only one, very heavy ion system.

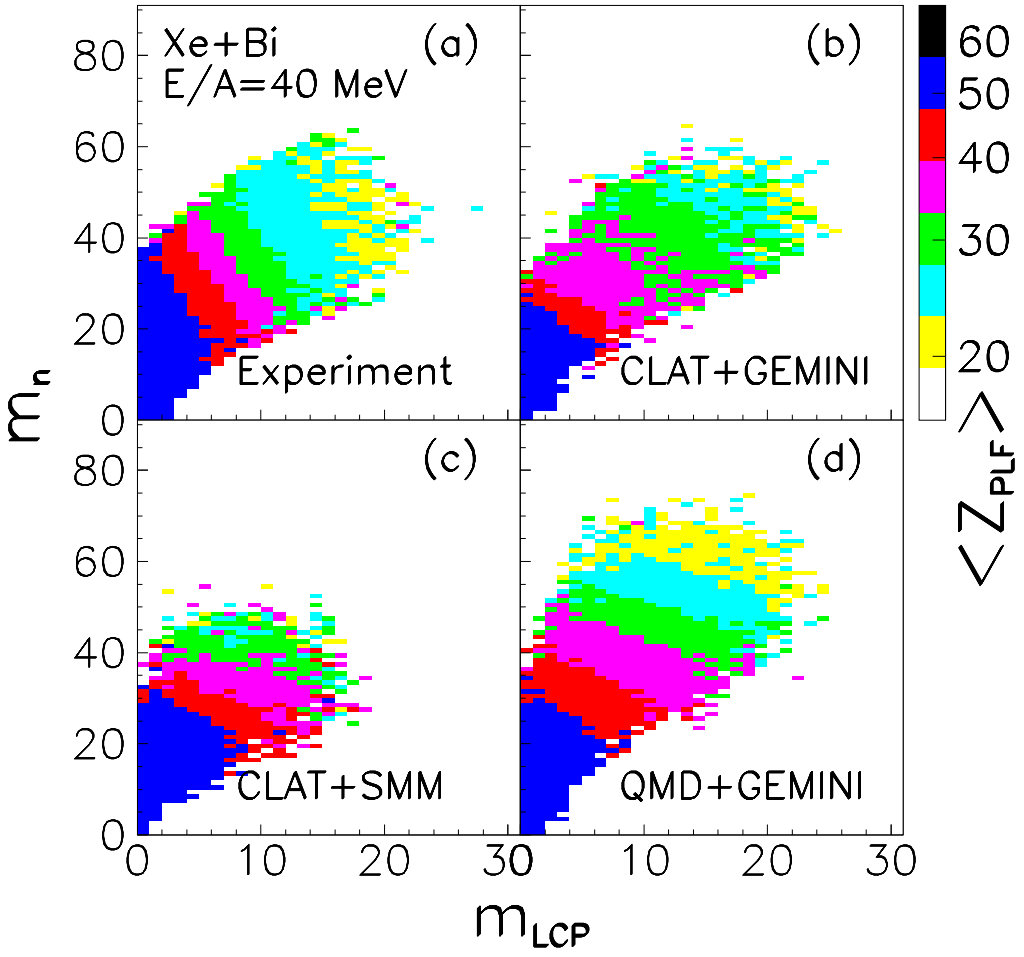

FIG. 5: (Color online) Logarithmic contour plot of average atomic number of the PLF, $< Z_{PLF} >$, as a function of associated neutron and LCP multiplicities, as predicted for the $^{136}Xe + ^{209}Bi$ reaction at E/A = 40 MeV by multi-step simulation calculations using codes CLAT and GEMINI (top row), CLAT and SMM (middle row), and QMD and GEMINI (bottom row).

This work was supported by the U.S. Dept. of Energy - Grants No. DE-FG02-88ER40414, DE-FG02-87ER-40316, and DE-FG02-88ER-40406, the Polish Ministry Of Science and Higher Education grant No. N N202 035636, and the M. Skłodowska-Curie Fund MEN/DOE-97-318.

---

[1] J. Wilczyński, Phys. Lett. **47B**, 124 (1973).

[2] W.U. Schröder, *Proc. Int. Worksh. Multifragmentation and Rel. Topics*, (R. Bougault et al., Edts.), INFN Conf. Proc. Vol. 91, pp. 303-335 (2005).

[3] C.P. Montoya et al., Phys. Rev. Lett. **73**, 3070 (1995).

[4] J.Tõke, B. Lott, S.P. Baldwin, B.M. Quednau, W.U. Schröder, L.G. Sobotka, J. Barreto, R.J. Charity, D.G. Sarantites, D.W. Stracener, and R.T. DeSouza, Phys. Rev. Lett. **75**, 2920 (1995).

[5] S. Hudan, R. Alfaro, B. Davin, Y. Larochelle, H. Xu, L. Beaulieu, T. Lefort, R. Yanez, R. T. de Souza, R. J. Charity, L. G. Sobotka, T. X. Liu, X. D. Liu, W. G. Lynch, R. Shomin, W. P. Tan, M. B. Tsang, A. Vander Molen, A. Wagner, and H. F. Xi, Phys. Rev. **C71**, 054604 (2005).

[6] J. B. Elliott, L. G. Moretto, L. Phair, G. J. Wozniak, L. Beaulieu, H. Breuer, R. G. Corteling, K. Kwiatkowski, T. Lefort, L. Pieńkowski, et al., Phys. Rev. Lett. 88, 042701 (2002).

[7] W. Skulski, J. Tõke, and W.U. Schröder, Phys. Rev. C 59, 2130R (1999)

[8] J. Bondorf et al., Phys. Rep. 257, 133 (1995).

[9] D.H. E. Gross, Phys. Rep. 279, 119 (1997).

[10] W. A. Friedman, Phys. Rev. Lett 60, 2125 (1988).

[11] F. Bocage et al., Nucl. Phys. A 676, 391 (2000).

[12] B. Davin et al., Pys. Rev. C 65, 064614 (2002).

[13] J. Colin et al., Phys. Rev. C 67, 064603 (2003).

[14] S. Piantelli et al., Phys. Rev. Lett. 88, 052701 (2002).

[15] E. de Filippo et al., Phys. Rev. C 71, 044602 (2005).

[16] D. W. Stracener et al., Nucl. Instr. and Meth. **A294**, 485 (1990).

[17] W. U. Schröder, REPORT DOE/ER/79048-1, 1995.

[18] W. Gawlikowicz, J. Tõke, and W.U. Schröder, Nucl.Instr. and Meth. **A491**, 181 (2002).

[19] W. U. Schröder et al., Nucl. Science Research Conf. Series, Vol.11, 255 (1986).

[20] J. Randrup, Nucl. Phys. **A307**(1978)319; **A327**(1979)490; **A383**, 468 (1982).

[21] J. Łukasik et al., Phys. Rev. **C55**, 1906 (1997).

[22] B.A. Li, L.-W. Chen, C. M. Ko, Physics Reports **464**, 113 (2008).

[23] R. J. Charity et al., Nucl. Phys. **A483**, 391 (1988).

[24] W. Gawlikowicz, Acta Phys. Pol. **28**, 1687 (1997).

[25] J. Poitou and C. Signarbieux, Nucl. Instr. and Meth. **114**, 11 (1974).

[26] U. Jahnke, G. Ingold, D. Hilscher, M. Lehmann, E. Schwinn, P. Zank, Phys. Rev. Lett. **57**, 190 (1986)

[27] J. Tõke, D.K. Agnihotri, W. Skulski, and W.U. Schröder, Phys. Rev. **C63**, 024604 (2001).

[28] W. U. Schröder and J. R. Huizenga, Treatise on Heavy-Ion Science Science, (D.A. Bromley, Editor), Vol.2, 113 (1984).

[29] E. Le Gentil et al., Phys. Rev. Lett. **100**, 022701 (2008) .